Journal of Materials Chemistry C

Enhanced protonic conductivity and IFET behavior in individual proton-doped electrospun chitosan fibers

Journal:	*Journal of Materials Chemistry C*
Manuscript ID	TC-ART-05-2019-002452.R1
Article Type:	Paper
Date Submitted by the Author:	08-Jul-2019
Complete List of Authors:	Lee, Woo-Kyung; US Naval Research Laboratory, Chemistry Pietron, Jeremy; Naval Research Laboratory, Chemistry Division Kidwell, David; US Naval Research Laboratory Robinson, J.; US Naval Research Laboratory, McGann, Christopher; U.S. Naval Research Lab, Chemistry Sheehan, Paul; Naval Research Laboratory, Department of Chemistry Mulvaney, Shawn; Naval Research Laboratory, Chemistry

Enhanced protonic conductivity and IFET behavior in individual proton-doped electrospun chitosan fibers

Woo-Kyung Lee,[*a] Jeremy J. Pietron,[a] David A. Kidwell,[a] Jeremy T. Robinson,[b] Christopher L. McGann,[c] Paul E. Sheehan[a] and Shawn P. Mulvaney[a]

[a]*Chemistry Division, U.S. Naval Research Laboratory, Washington, DC, 20375 USA*

[b]*Electronics Science and Technology Division, U.S. Naval Research Laboratory, Washington, DC, 20375 USA*

[c]*American Society for Engineering Education Postdoctoral Fellow, Chemistry Division, U.S. Naval Research Laboratory, Washington, DC 20375, United States*

ABSTRACT: A major challenge for biomedical science is developing materials and processing methods to enable creation of devices that can meaningfully translate signals between biology and electronics. Protonics-based devices—devices analogous to electronic devices but which use protons as charge carriers instead of electrons—are a promising strategy for such translation. Proton-conductive materials (PCMs)—the media through which protons are transported in such devices—are an element ripe for improvement, since they dominate the performance of protonic devices. We investigate protonic devices comprising sub-micrometer diameter, chitosan-fiber PCMs and palladium hydride (PdH_x) protodes, the proton-injecting contact, to analyze how proton transport depends on the chemistry and ordering of the PCM. Current–voltage (I–V) measurements of single fiber-based devices under hydrogen atmospheres show that fibers electrospun from

trifluoroacetic acid (TFA) solutions feature substantially higher proton conductivity, up to two orders of magnitude, compared to chitosan PCM films cast from acetic acid solutions. We further used digital simulation of the I–V data to elucidate the electrochemical and electrical processes that control device operation. The hydrogen oxidation reaction kinetics of the protode interfaces with the electrospun chitosan fibers agree well with those reported previously. Using X-ray photoelectron spectroscopy (XPS), we observed that single chitosan fibers spun from TFA solutions are more highly proton-doped than chitosan cast from acetic acid. Furthermore, I–V measurements on electrospun chitosan fibers vs. spin-cast chitosan films, both derived from TFA solutions, reveal that electrospun chitosan fibers yields ~10-fold higher proton conductivity, suggesting that local polymer ordering within the electrospun fibers further enhances proton transport for chitosan PCMs. Finally, devices fabricated from single doped chitosan fibers behave as ionic field effect transistors (IFETs) when under a contact gate bias established with a conducting probe AFM tip. Switching characteristics are tuned by the gate bias, with proton conduction of a single fiber increasing by over an order of magnitude under negative bias. The switchable ion currents and enhanced conductivity of the chitosan fiber-based PCMs comprise a means of establishing spatiotemporal control over ionic communication between protonic devices and adjacent biological cells and membranes.

KEYWORDS: Proton-conductive materials, chitosan, electrospinning, helium ion microscope, ionic field effect transistors (IFETs)

Introduction

Compatibility at the biotic-abiotic interface is critical to the performance of biomedical devices, biofuel cells, environmental sensor systems, and other related technologies. Communication

between the biotic and abiotic components is a common point of failure because the languages of biology and electronics differ: biology communicates via ionic or small-molecule signaling, whereas electronics employs electron conduction. Monitoring ionic biological processes has been achieved with many different classes of sensors; however, controlling or actuating biological processes via controlled (spatially and temporally) ionic release remains substantially less developed. Discoveries in protonics[1,2] suggests that the controlling aspect of communication can be more successfully bridged. Indeed, we are in the process of harnessing protonic communication between biology and protonic devices to actuate cellular networks in our laboratory and recognize that a more robust communication signal would be of significant benefit. Rather than traditional electrophysiology methods, which typically use large currents and voltages to actuate the desired biological response, protonic devices translate electric currents into ionic currents at the interface between the device and the biological medium. The protonic interface enables generation of protons at a protode, often a palladium hydride (PdH_x) electrode controlled with a standard electronic potentiostat. Protons are released at the protode via the electrochemical hydrogen-oxidation reaction (HOR), and can transfer to protonic conductive materials, with which the protode is in contact.[3] The PCM can then act as a relay to the biological medium in biotechnology applications, for example in the control of proton transport by gramicidin across lipid bilayer membranes,[4] the control of the pH-dependence of glucose and alcohol dehydrogenases,[5,6] and in conjunction with light-activated deltarhodopsin in the conversion of protonic currents to electronic currents[7] or can even itself act as an artificial synapse.[8]

Chitosan has been studied extensively for use in a broad range of biomedical applications such as bio-filters,[9] drug delivery systems,[10] and wound dressing[11] due to its biocompatibility and biodegradability.[12] The natural form of chitosan conducts ions relatively poorly[3]; however,

modification with acid can enhance its proton conductivity sufficiently to operate protonic devices.[13,14] Nevertheless, overall performance of protonic devices are limited by conductivity and, consequently, chemical functionalization strategies such as modification with toluene sulfonic acid to make maleic chitosan[14,15] and doping with various salts[16-18] have been pursued.

Here, we examine the impact of polymer organization on proton mobility as induced by electrospinning. The high shear rates produced during the electrospinning of fibers can order the polymer at the nanoscale.[19] We hypothesize that ordered domains should accelerate ion transport along the longitudinal axes of the fibers.[20-22] Previously, Gu *et al.* has shown that the electrical conductivity of electrospun, aligned chitosan/polyaniline blend fibers was ~91% higher than that of randomly deposited fibers.[23] Lu *et al.* has reported thermal conductivity of electrospun, aligned polyethylene oxide fibers was increased ~150 times over bulk polymer.[24]

A second materials constraint for such devices is the PCM's amenability to microfabrication. Actuating biological responses in a highly localized manner, whether in a large, multi-celled organism or in populations of cultured cells and cell networks will require protonic devices that function on the micrometer-scale. Chitosan nanofibers are a promising material to realize such miniaturized PCM geometries.[14] Electrospun chitosan fibers have been used in textile mats and as fibrous bundles featuring large surface areas and high porosity.[12]

In the present study, to examine these two critical aspects of protonic interface design (improvement of chitosan conductivity through electrospinning and miniaturization of the chitosan-based proton-conducting interface), we fabricated protonic devices with electrospun chitosan fibers and employed a helium ion microscope (HIM) to isolate individual fibers deposited across Pd protodes. We then measured the I−V behavior at these single-fiber devices under hydrogen (H_2) atmospheres and analyzed the transformation of electric current into a protonic

current via the electrochemical hydrogen oxidation reaction (HOR) at the protode (PdH_x)/chitosan interfaces using digital simulation. This multifaceted electroanalytical approach yields good agreement in conductivity values acquired across the different analysis methods and enables us to assign the origins of the enhanced ionic conductivity to a combination of enhanced proton doping and domain ordering in the electrospun fibers. Finally, we observe both further enhanced conductivity as well as switching behavior in individual electrospun fibers when applying a negative gate bias to the fiber configured as the conducting channel in an ionic field effect transistor (IFET). These observations suggest that the doped chitosan fibers are excellent candidates for delivering ions to biological cells and interfaces with good spatiotemporal control.

Experimental Details

Fabrication of protonic device

Photolithography was used to define the metal protodes used for electrical measurements of the chitosan fibers. The protodes consisted of a 5 nm Ti sticking layer and 30 nm Pd metal layer that were deposited onto a 100nm SiO_2/Si substrate. After metal patterning, liftoff, and substrate cleaning, the chitosan fibers were electrospun onto the metallized substrates.

Electrospinning of chitosan

Chitosan was acquired from TCI America (Portland, OR) and had a viscosity range of 50-100 mPa s for a 0.5 wt% solution dissolved in 0.5% acetic acid. Reagent grade methylene chloride (DCM) and trifluoroacetic acid (TFA) were acquired from Fisher Scientific (Waltham, MA) and Sigma Aldrich (St. Louis, MO), respectively. Aligned chitosan fibers were deposited via electrospinning onto substrates attached to a rotating drum using protocols adapted from Ohkawa,

et al.[25,26] Briefly, 350 mg of chitosan was dissolved overnight in 10 mL of a 70/30:TFA/DCM mixture at room temperature with mixing. A syringe pump (New Era Pump Systems Farmingdale, NY) ejected chitosan solution at 20 μL/min rate from a 1 mL syringe equipped with a 22 Ga. blunt end needle using a voltage of 15 kV and at a distance of 15 cm from the rotating drum target. Substrates were attached to the drum using copper tape and rotated at 1000 RPM; samples were deposited for no longer than two minutes.

Isolation of a single chitosan fiber devices

A helium ion microscope (HIM) was utilized to isolate a single chitosan nanofiber between Pd protodes by cutting all other fibers that span the protodes. The He ion beam current was set at ~10 pA and exposed at a dose of 0.5 nC/μm^2. The complete cut of a single chitosan fiber took 1-2 min under our experimental conditions.

Characterization of electrical and protonic conductivity

A probe station with custom-built environmental controlled chamber and Keithley 4200 semiconductor analyzer was used to characterize electrical properties of protonic devices. The devices was characterized under 0%, 75% RH without H_2, and 75% RH with 10% H_2 atmosphere. The relative humidity was controlled by bubbling nitrogen gas or 10%H_2/90% N_2 gas.

Digital simulation

Digital simulation of current–voltage (I–V) data was performed using Digisim® 3 digital simulation software (BASi), using parameters specified for each chitosan fiber-based protonics device as described in detail in the Supplementary Information.

Ionic Field Effect Transistors (IFETs)

An atomic force microscope (multimode AFM, Bruker) with custom-built environmental controlled chamber was used to characterize chitosan fiber IFETs. For a gate configuration, Au-coated, tip-less AFM probe was utilized to increase contact area at the interface between chitosan fiber and probe. The Pd electrodes and the probe were securely wired into the source-measurement units of Keithley 4200 semiconductor analyzer to measure IV characteristics by applying DC voltages to the probe. IFETs were characterized under 0%, 75% RH without H_2, and 75% RH with 10% H_2 atmosphere. The relative humidity was controlled by bubbling nitrogen gas or 10%H_2/90% N_2 gas.

Results and Discussion

Casting and cutting single chitosan fibers with low- and sub-micrometer diameters

Electrospun, maleic chitosan nanofibers were previously studied by Zhong *et al.*[14] They reported enhanced protonic conductivity deriving from chitosan functionalization; however, those fibers were neither oriented in a directionally-controlled manner, nor was their number density controlled, making quantitating conductivity at individual fibers impossible. To measure proton conductance of single chitosan fibers, we deposited low number densities of oriented chitosan fibers on Pd electrodes, which form PdH_x protodes under H_2-containing atmospheres (Fig. 1a). We controlled the concentration of chitosan in solutions and deposition times and used a rotating drum to control fiber number density and to align the fibers. Individual fiber diameters achieved using our deposition conditions ranged from < 100 nm to ~1200 nm (Fig. 1b). The average fiber diameter was approximately 400 nm.

We employed the ion beam of a helium ion microscope (HIM, Zeiss) to image and isolate a

single fiber between protodes. This approach enables us to precisely control the length of a single fiber for conductivity measurements and electrochemical simulations without depositing other potentially conductive materials on the fiber. Our approach with the HIM comprises: (1) cutting fibers lying across the protode pairs until only a single, conductive path remains; and (2) cutting the length of the remaining fiber to control the contact area with the protodes and the total length of the proton conducting pathway. Fig. 2a shows a protonic device with 20 μm total fiber length spanning a 5 μm channel, with 7.5 μm of overlap at each protode to create source and drain contacts.

Resistivity/conductivity measurements at single chitosan fibers

We measured the conductivity of single-fiber devices in a humidified (75% relative humidity (RH)) nitrogen ambient, both without and with hydrogen (H_2, 10% fraction; Fig. 2)). Under 10% H_2 (red curve), the current response in the I–V curves is 10-fold higher (~± 100–150 pA at ± 1 V) than that measured under humidified N_2 alone (~± 10–15 pA at ± 1 V). The resistivity values of single chitosan fibers in 10% H_2 (Fig. 2c) were evaluated from I–V curves taken under humidified H_2/N_2, with the data acquired under humidified N_2 subtracted as background. The average resistivity (ρ) for a series of wires was found to be 6.2×10^4 Ω·cm, corresponding to a proton conductivity ($\sigma = 1/\rho$) of 1.6×10^{-5} S·cm^{-1}. Notably, we found no clear dependence of the resistivity of fiber dimensions such as diameter, channel length, or *apparent* contact area with the protodes (as estimated visually by the spatial overlap between the chitosan fiber and the protode). The actual area of intimate physical contact between the chitosan fiber and the protode is difficult to estimate. We attempted electrochemical impedance spectroscopy (data not shown) to better differentiate the nanofiber–protode contacts in the different samples, but poor signal/noise ratios made the data

impossible to interpret. As a control experiment to measure possible substrate conductivity, we severed all fibers in the channel between protodes by HIM milling, and subsequently measured no resistance change in the presence or absence of hydrogen upon applying voltage sweeps between the PdH_x protodes (See Supplementary information, SI. 1). The absence of measurable currents indicates that there are no substantial electronic or ionic conduction pathways on the surfaces of the fabricated Pd devices themselves.

Enhanced conductivity in electrospun chitosan fibers: effects of H^+ doping versus nanoscale ordering

A primary motivation for producing chitosan fibers was to determine if proton transport in chitosan can be enhanced through morphology, both from a reduced physical size (*i.e.*, scale), as well as through the formation of ordered nanoscale domains of the chitosan polymer itself. It is known that shear forces generated during electrospinning can create ordered domains in polymeric materials, as previously described.[20-24] Unfortunately, directly imaging the nanoscale ordering is nearly impossible as neither our HIM images (see Supplementary information, SI. 2) nor the previously published TEM and SEM images of chitosan nanofibers have enough resolution to demonstrate the ordering, especially in the fiber's interior.[27] However, electrical measurement provided insight. Our single chitosan fiber-based devices feature chitosan conductivities that are two orders of magnitude higher than those measured previously for chitosan films between Pd protodes.[3] The resistivity previously measured at chitosan films (spun from 30% aqueous glacial acetic acid) ranged from 2×10^7–1×10^8 Ω·cm,[3] while data for our electrospun chitosan fiber (Fig. 2) yield an average of $\sim 6 \times 10^4$ Ω·cm—roughly a factor of 1000× less resistive than the chitosan films. However, the chitosan nanofibers in the present study were spun from chitosan solutions

containing 70% trifluoroacetic acid (TFA) and 30% dichloromethane. The acidity of TFA (pKa = 0.22) is substantially higher than that of acetic acid (pKa = 4.7), which would result in an approximately 500-fold higher H^+ concentration in TFA-derived PCMs under ideal conditions—that is, where the dilute solution approximation is appropriate for the electrospun and cast chitosan PCMs respectively, *and* the resultant degree of hydration of the doped chitosan nanofibers and films is approximately the same. A second equilibrium that requires consideration—beyond that of the protons and their source conjugate bases—acetate and trifluoracetate—is that between protons and nitrogen groups in chitosan. While we can only approximately estimate the differences between the proton concentrations in the TFA- and acetic acid- derived PCMs using pKa values, the differences in measured conductivity are in good agreement with the estimates.

Chemical comparison of proton doping by TFA and acetic acid

For direct observation of the degree of protonation of the TFA- and acetic acid-derived PCMs, we turned to X-ray photoelectron spectroscopy (XPS). Fig. 3 shows XPS of the N 1s and F 1s core levels for films cast from chitosan solutions made with (i) acetic acid/H_2O, and (ii) 70% TFA/30% dichloromethane. Notably, the N 1s peaks from the TFA-derived chitosan films (Fig. 3a) are substantially more protonated than chitosan films from the acetic acid solution (Fig. 3c). At the same time, the F 1s spectrum (Fig. 3b) clearly shows fluorine in chitosan films spun from TFA solutions (coming from TFA residues), whereas no F 1s signature is found in chitosan films cast from acetic acid solutions, as expected (Fig. 3d). We note that even though TFA and acetic acid are considered to be volatile acids, they persist under the high vacuum conditions ($< 10^{-8}$ Torr) for several hours.

This chemical analysis helps to identify a pathway through which TFA residues in chitosan films and fibers play a role in proton conductivity— through protonating amine groups on chitosan side chains to create bound NH_3^+ groups. The peak area analysis of N 1s and F 1s from TFA-doped chitosan film shows the ratio between fluorine vs protonated nitrogen is 3, suggesting that all the TFA residues are associated the amine group, *i.e.* proton doping. Knowing that TFA residues remain after film formation, we apply sequential treatments to further remove these residues via: (i) exposure to aqueous NaOH (1% solution) (ii) rinsing in acetone, and (iii) drying in vacuum. The XPS analysis of the N 1s spectrum reveals deprotonation of the nitrogen group and removal of trifluoroacetate after this treatment (See Supplementary information, SI. 3). Subsequent I–V measurements on the deprotonated devices under 10% H_2 reveal a complete loss of conductivity, which further supports the role of residual TFA in proton doping (See Supplementary information, SI. 4). The detailed proton conductivity mechanism is likely controlled by a Grotthuss-type water wire mechanism[1] mitigated by the acid–base equilibrium between the amine groups in the chitosan side chains and the water present in the fibers or films.

Separating the variables, part 1: Comparing TFA-derived chitosan films to acetic-acid derived chitosan films

While the XPS data show that the chitosan nanofibers spun from TFA have more highly protonated nitrogen groups than those spun from acetic acid (Figs. 3a, c), quantifying the concentrations of mobile protons in the two PCMs—derived from different solutions and processed differently, *i.e.* as electrospun fibers in one case and as spin-cast films in another—is more complex. More direct control samples were generated by casting chitosan films from each

chitosan solution and then processing them in parallel into devices (Fig. 3e). After drying, chitosan films cast from TFA solutions are 20× more conductive in 10% H_2 atmospheres than those cast from acetic acid solutions (Fig. 3f). Specifically, we derive from the I–V data (Fig. 3f), the areas of the electrodes, and the 8-μm gaps as the conducting distance yields resistivity (ρ) values of ~6.3×10^5 Ω·cm for the TFA and ~1.2×10^7 Ω·cm for the acetic acid-derived chitosan films. This difference in conductivity is substantially less than a proton-concentration ($[H^+]$)-normalized value that might be predicted by the 500-fold difference in $[H^+]$ alone as estimated from the pKa values of the acids. The dilute solution pK_a-based approximation, however, may not be valid for the films; additionally, as described in terms of the XPS data, the acid–base interactions of protons with nitrogen groups in the chitosan fibers and films must be considered. Regardless of the precise reason for the conductivity differences (doping levels, acid–base equilibria), when comparing both films, the TFA-derived chitosan is ~20× more conductive.

Separating the variables, part 2: Comparing TFA-derived chitosan films to TFA-derived chitosan fibers by multiple methods

Having identified the differences between chitosan films derived from different acidic solutions, we attempt to deconvolute the effects of electrospinning on ionic conductivity in TFA-derived chitosan PCMs. The ρ values for the TFA-doped chitosan fibers are ~10-fold lower (*i.e.*, higher conductivity) as compared to TFA-doped chitosan films when analyzing the slopes of the linear portions of the I-V data. We hypothesize that this enhanced conductivity in electrospun TFA-doped chitosan arises from enhanced ion transport in nanoscale ordered polymer domains. Those domains are formed due to the shear forces that occur during the electrospinning process.[20,22] We cannot eliminate the possibility that the TFA-derived wires and films retain

different amounts of residual water and TFA after processing, but they are processed as nearly identically as possible before I–V measurements are made.

To further validate our resistivity values, we applied electrochemical digital simulation to I–V data from several TFA-doped chitosan nanofiber devices. The key electrochemical process controlling currents at PdH_x protodes in H_2 atmospheres is the HOR, which occurs in two steps, including the dissociative adsorption of H_2 to form surface and sub-surface adsorbed H_x species (Eq. 1: this step is typically rate-determining in the HOR at Pd[28]), and the subsequent oxidation of the adsorbed hydrogen atom to yield a proton (Eq. 2):

$$Pd + 1/2\,H_2 \rightarrow PdH_x \qquad [1]$$

$$PdH_x \rightarrow Pd + H^+ + e^- \qquad [2]$$

Simulated electrochemical data based on electrochemical Eq. 1 fit very well with background-subtracted device data (Fig. 4). The resistivity value extracted for the simulated data in Fig. 4 is $9.8 \times 10^4\ \Omega\cdot$cm, which is in excellent agreement with the value of $1.2 \times 10^5\ \Omega\cdot$cm derived from simple analysis of the linear portion of the experimental I–V data for the same device. Additionally, digital simulation yields an electrochemical rate constant (k) for the HOR [Eq. 1] at this device of 2×10^{-5} cm$\cdot$s^{-1}, essentially identical to the values of k determined for the HOR at chitosan/PdH_x protodes in our previous study.[3] The estimated differences in proton concentration in the TFA- and acetic acid-derived chitosan films is incorporated in the digital simulation; thus the nearly identical rate constants derived from the fits to the experimental data suggest the electrochemical kinetics do not change significantly across the differently-doped chitosan PCMs. Simulation of several single fibers produced similar good fits (See Supplementary information, SI. 5). Conductivity data and electrochemical rate constants for several chitosan nanowires, along with the geometric

dimensions of each nanowire, are compiled in Table I.

Finally, the extracted ρ value for the acetic acid-doped chitosan film measured here (1.2×10^7 Ω·cm) is within a factor of two of the ρ values extracted using digital simulation of I–V data (5.9×10^6 Ω·cm) obtained for acetic acid-derived chitosan films in our previous study.[3] In particular, the protodes in the previous study were of different geometries than those used in this study; none the less, the good agreement for resistivity values obtained between these different samples provides confidence to this analytic approach in general. We note that TFA was used in the present study as an example of a highly proton-donating dopant that could be clearly contrasted with acetic acid to characterize the effects of doping on model chitosan-based protonic interfaces. As TFA can be toxic to some living cells and tissues, the choice of dopant must be carefully considered when designing protonic interfaces that will come in direct contact with living systems.

Ionic field-effect transistor made from individual chitosan fibers

To further characterize our single chitosan fiber we tested proton transport characteristics in the presence of an electric field by applying DC gate bias directly to a fiber *via* Au-coated AFM probe as a gate (See Supplementary information, SI. 6). To ensure electrical contact at the interface of a fiber and Au-coated AFM probe, we employed a tip-less probe. The probe was placed in contact the fiber using contact mode AFM without scanning an area. This approach creates a direct-contact, top-gated field-effect transistor, therefore, it does not require additional dielectric layer such as SiO_2 for device operation. Fig. 5a shows the measurement of a current between source and drain PdH_x protodes with gate bias varied from -20V to +20V in +5V steps under 10% H_2 / 90% N_2 at 75% RH. Our test device was built from a fiber with a 1000 nm diameter spanning a 22.4 μm channel length. The Au-coated AFM probe contacted the fiber approximately at the center of

the channel. As in the single fiber conductivity measurements described in the sections above, all other fibers across electrodes were cut with the HIM before taking I–V data to ensure measurement across only a single fiber.

Ionic FET behavior at chitosan-based protonics devices has been described previously.[14] When applying a negative gate bias, the interface between the chitosan proton conducting channel and the gate acts as a capacitor that accumulates negative charge. To compensate this excess negative charge, protons are injected into the chitosan PCM from the PdH_x source protode, increasing carrier concentration.[14] In the present study, applying a -20V gate bias decreases resistivity in single chitosan fibers from the typical values of $\sim 10^5$ Ω·cm under zero bias conditions (Table I) to 8.6×10^3 Ω·cm in the chitosan fiber-based IFET—i.e. producing an order-of-magnitude increase in proton conductivity. Moreover, proton conduction can be controlled by varying negative gate bias, producing increasing proton currents with increasing negative bias (Fig. 5b). Applying positive gate bias decreases proton conduction, as the excess positive charge at the gate–proton channel capacitive interface under positive bias inhibits injection of protons into the chitosan channel by the PdH_x source protode (Fig. 5b). As shown in Fig. 5a, I–V curves acquired at positive gate bias are similar to those obtained at 0V bias. Figure 5b clearly shows the switching characteristics of proton transport by gate sweep (±20V) at 0.5V of source–drain (S–D) voltage. In our measurement conditions, the on/off ratio was ~3.5. There is essentially no field-effect in the absence of H_2 flow (black curve), as proton concentration in the channel diminishes substantially and the small device currents are largely due to small parasitic water oxidation and reduction currents at the protodes,[3] Thus, the IFET behavior observed is almost exclusively due to modulation of proton transport in individual chitosan fibers by top-gate bias. We note that there is a significant contribution from leakage current (non-zero current at zero S–D voltage), especially

at negative gate bias, presumably due to water splitting while applying high electric field under such a high relative humidity.[29] A more detailed study of IFET behavior at single electrospun chitosan fibers is currently underway.

Conclusions

Protonics devices employing electrospun, TFA-doped chitosan fibers as the proton-conductive materials (PCMs) exhibit enhanced proton conductivity over devices based on chitosan films deposited from acetic acid solutions. The enhanced conductivity arises partially from higher proton doping levels achieved by more acidic TFA compared to casting from acetic acid. Proton conductivity is also higher in electrospun TFA-derived chitosan fibers relative to that measured in chitosan films cast from identical TFA/chitosan solutions, suggesting that nanoscale ordering of the fibers further enhances conductivity. However, because imaging the local ordering of domains in individual chitosan fibers fabricated for the present study was not possible, other factors—such as different diffusion profiles arising at microscale interfaces, and variation in hydration of chitosan interfaces featuring different geometries—cannot be ruled out as full or partial causes of the increase in conductivity. Regardless of the exact driver of the enhanced conductivity in the electrospun fibers, the fabrication of functional micron-scale protonics devices demonstrated here shows that miniaturized protonics devices are feasible. Furthermore, individual, doped chitosan fibers exhibit IFET behavior in top-gated configuration, demonstrating that ionic currents in these miniaturized polymeric protonic devices can be controlled with good precision. The enhanced protonic conductivity and the FET-like switchability achievable in the micron-scale electrospun doped chitosan fibers comprise a means to incorporate ion current delivery in protonics large enough to deliver robust biological responses with good spatiotemporal control.

Conflicts of interests

There are no conflicts to declare.

Acknowledgements

This research was supported by the Office of Naval Research (ONR) through the NRL Nanoscience Institute.

Notes and references

1 Miyake, T.; Rolandi, M. Grotthuss mechanisms: from proton transport in proton wires to bioprotonic devices. *J. Phys-Condens. Mat.* **2016**, *28*, 023001.
2 Hemmatian, Z.; Miyake, T.; Deng, Y. X.; Josberger, E. E.; Keene, S.; Kautz, R.; Zhong, C.; Jin, J. H.; Rolandi, M. Taking electrons out of bioelectronics: bioprotonic memories, transistors, and enzyme logic. *J. Mater. Chem. C* **2015**, *3*, 6407-6412.
3 Robinson, J. T.; Pietron, J. J.; Blue, B.; Perkins, F. K.; Josberger, E.; Deng, Y.; Rolandi, M. Electrical and electrochemical characterization of proton transfer at the interface between chitosan and PdHx. *J. Mater. Chem. C* **2017**, *5*, 11083-11091.
4 Hemmatian, Z.; Keene, S.; Josberger, E.; Miyake, T.; Arboleda, C.; Soto-Rodriguez, J.; Baneyx, F.; Rolandi, M. Electronic control of H+ current in a bioprotonic device with Gramicidin A and Alamethicin. *Nat. Commun.* **2016**, *7*, 12981.
5 Deng, Y. X.; Miyake, T.; Keene, S.; Josberger, E. E.; Rolandi, M. Proton mediated control of biochemical reactions with bioelectronic pH modulation. *Sci. Rep.* **2016**, *6*, 24080.
6 Miyake, T.; Josberger, E. E.; Keene, S.; Deng, Y. X.; Rolandi, M. An enzyme logic bioprotonic transducer. *APL Mater.* **2015**, *3*, 014906.
7 Soto-Rodriguez, J.; Hemmatian, Z.; Josberger, E. E.; Rolandi, M.; Baneyx, F. A Palladium-Binding Deltarhodopsin for Light-Activated Conversion of Protonic to Electronic Currents. *Adv. Mater.* **2016**, *28*, 6581.
8 Zhu, L. Q.; Wan, C. J.; Guo, L. Q.; Shi, Y.; Wan, Q. Artificial synapse network on inorganic proton conductor for neuromorphic systems. *Nat. Commun.* **2014**, *5*, 3158.
9 Cooper, A.; Oldinski, R.; Ma, H. Y.; Bryers, J. D.; Zhang, M. Q. Chitosan-based nanofibrous membranes for antibacterial filter applications. *Carbohyd. Polym.* **2013**, *92*, 254-259.
10 Agnihotri, S. A.; Mallikarjuna, N. N.; Aminabhavi, T. M. Recent advances on chitosan-based micro- and nanoparticles in drug delivery. *J. Control. Release* **2004**, *100*, 5-28.
11 Jayakumar, R.; Prabaharan, M.; Kumar, P. T. S.; Nair, S. V.; Tamura, H. Biomaterials based on chitin and chitosan in wound dressing applications. *Biotechnol. Adv.* **2011**, *29*, 322-337.
12 Sun, K.; Li, Z. H. Preparations, properties and applications of chitosan based nanofibers fabricated by electrospinning. *Express Polym. Lett.* **2011**, *5*, 342-361.
13 Deng, Y. X.; Josberger, E.; Jin, J. H.; Roudsari, A. F.; Helms, B. A.; Zhong, C.; Anantram, M. P.; Rolandi, M. H+-type and OH--type biological protonic semiconductors and complementary devices (vol 3, 2481, 2015). *Sci. Rep.* **2015**, *5*, 2481.
14 Zhong, C.; Deng, Y. X.; Roudsari, A. F.; Kapetanovic, A.; Anantram, M. P.; Rolandi, M. A polysaccharide bioprotonic field-effect transistor. *Nat. Commun.* **2011**, *2*, 476.
15 Zhong, C.; Wu, J.; Reinhart-King, C. A.; Chu, C. C. Synthesis, characterization and cytotoxicity of photo-crosslinked maleic chitosan-polyethylene glycol diacrylate hybrid hydrogels. *Acta Biomater.* **2010**, *6*, 3908-3918.
16 Buraidah, M. H.; Teo, L. P.; Majid, S. R.; Arof, A. K. Ionic conductivity by correlated barrier hopping in NH4I doped chitosan solid electrolyte. *Physica B.* **2009**, *404*, 1373-1379.
17 Khiar, A. S. A.; Puteh, R.; Arof, A. K. Conductivity studies of a chitosan-based polymer electrolyte. *Physica B.* **2006**, *373*, 23-27.
18 Majid, S. R.; Arof, A. K. Proton-conducting polymer electrolyte films based on chitosan acetate complexed with NH4NO3 salt. *Physica B.* **2005**, *355*, 78-82.
19 Jiang, S. H.; Chen, Y. M.; Duan, G. G.; Mei, C. T.; Greiner, A.; Agarwal, S. Electrospun nanofiber reinforced composites: a review. *Polym. Chem.* **2018**, *9*, 2685-2720.

20 Garg, K.; Bowlin, G. L. Electrospinning jets and nanofibrous structures. *Biomicrofluidics* **2011**, *5*, 013403.
21 Jana, S.; Cooper, A.; Ohuchi, F.; Zhang, M. Q. Uniaxially Aligned Nanofibrous Cylinders by Electrospinning. *Acs Appl. Mater. Inter.* **2012**, *4*, 4817-4824.
22 Li, D.; Xia, Y. N. Electrospinning of nanofibers: Reinventing the wheel? *Adv. Mater.* **2004**, *16*, 1151-1170.
23 Gu, B. K.; Park, S. J.; Kim, C. H. Beneficial effect of aligned nanofiber scaffolds with electrical conductivity for the directional guide of cells. *J. Biomat. Sci-Polym. E.* **2018**, *29*, 1053-1065.
24 Lu, C. H.; Chiang, S. W.; Du, H. D.; Li, J.; Gan, L.; Zhang, X.; Chu, X. D.; Yao, Y. W.; Li, B. H.; Kang, F. Y. Thermal conductivity of electrospinning chain-aligned polyethylene oxide (PEO). *Polymer* **2017**, *115*, 52-59.
25 Ohkawa, K.; Cha, D. I.; Kim, H.; Nishida, A.; Yamamoto, H. Electrospinning of chitosan. *Macromol. Rapid Comm.* **2004**, *25*, 1600-1605.
26 Katta, P.; Alessandro, M.; Ramsier, R. D.; Chase, G. G. Continuous electrospinning of aligned polymer nanofibers onto a wire drum collector. *Nano Lett.* **2004**, *4*, 2215-2218.
27 Cooper, A.; Bhattarai, N.; Kievit, F. M.; Rossol, M.; Zhang, M. Q. Electrospinning of chitosan derivative nanofibers with structural stability in an aqueous environment. *Phys. Chem. Chem. Phys.* **2011**, *13*, 9969-9972.
28 Shao, M.H. Palladium-based electrocatalysts for hydrogen oxidation and oxygen reduction reactions. *J. Power Sources* **2011**, *196,* 2433–2444.
29 Deml, A. M.; Bunge, A. L.; Reznikov, M. A.; Kolessov, A.; O'Hayre, R. P. Progress toward a solid-state ionic field effect transistor. *J. Appl. Phys.* **2012**, *111,* 074511.

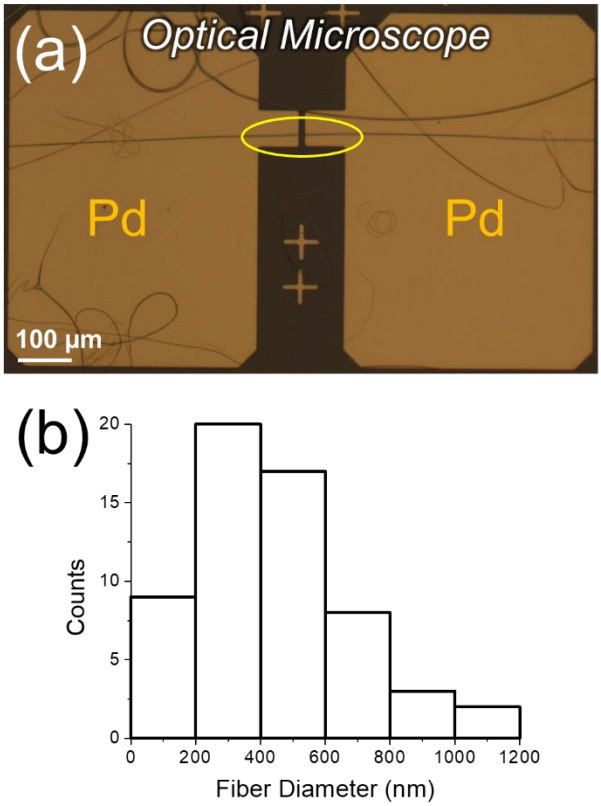

Fig. 1. Electrospun chitosan fiber deposited on Pd protodes with low densities; an individual fiber spanning the inner-electrode gap is highlighted by the yellow ring. (a) Optical micrograph of aligned chitosan fiber between pre-fabricated Pd protodes (b) the distribution of electrospun fiber diameters.

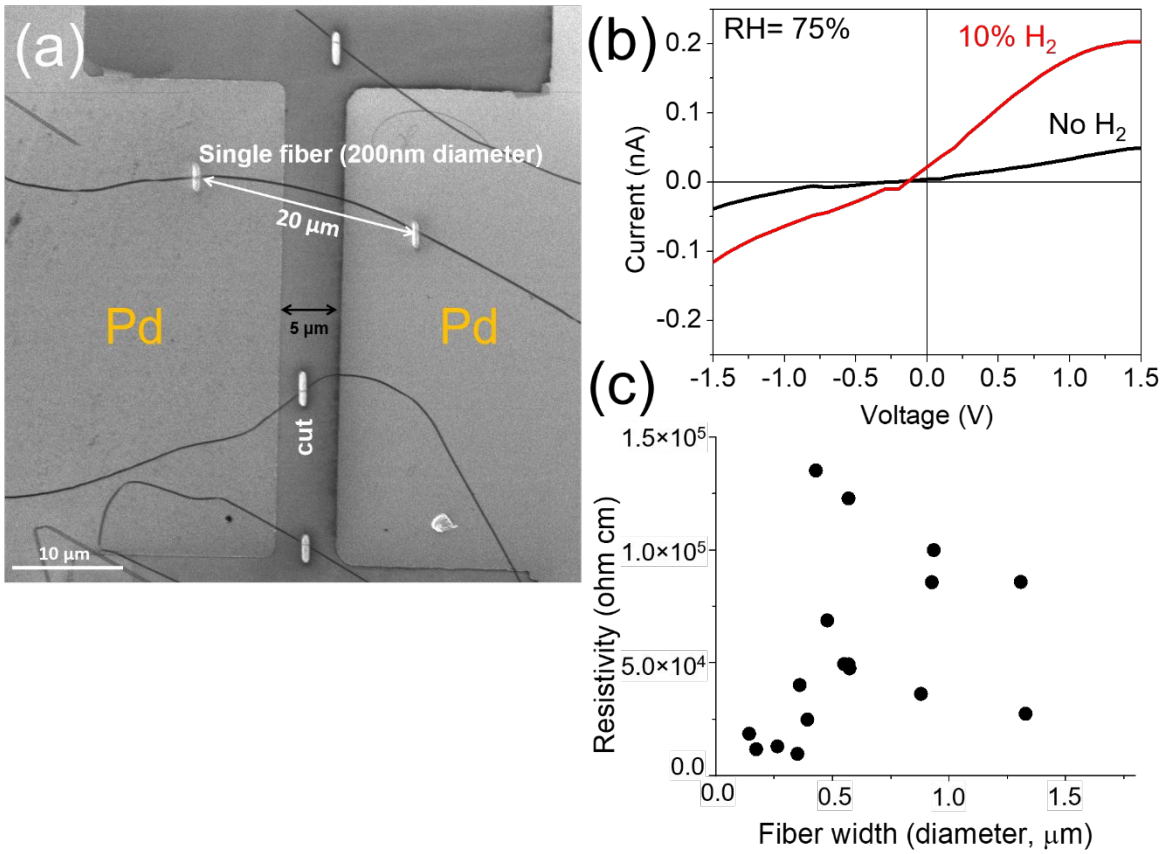

Fig. 2. Characterization of protonic conductivity of a single chitosan fiber: (a) single chitosan fiber between Pd protodes isolated by cutting with focused helium ion beam using the HIM; (b) current–voltage curve of a single chitosan fiber under 75% RH N_2 atmosphere in H_2-free conditions (black curve) and with 10% H_2 (red curve); (c) calculated resistivities of single chitosan fibers from measured dimensions (diameter and channel length). The R-squared value from a linear regression was 0.356, suggesting that there is no clear dependence between resistivity and fiber dimensions.

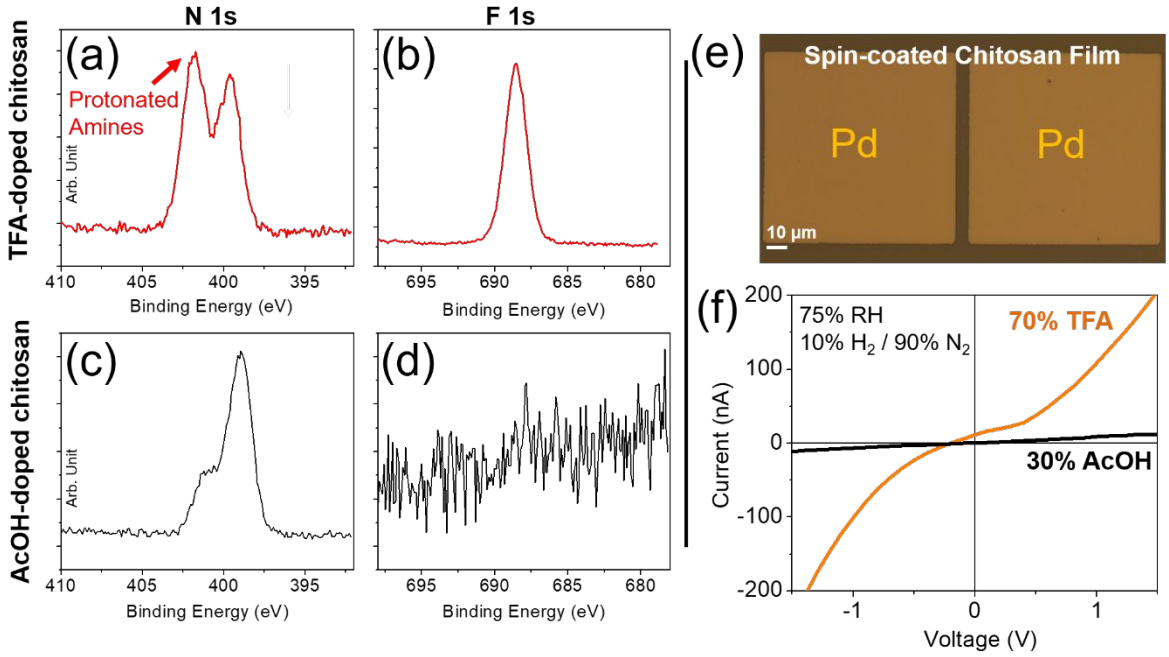

Fig. 3. XPS analysis and I–V measurements of spin-coated doped chitosan films from 70% TFA-30% DCM solution and 30% acetic acid solution (AcOH). (a-d) XPS analysis of TFA-doped chitosan film ((a) N 1s and (b) F 1s) and acetic acid-doped chitosan film ((c) N 1s and (d) F 1s). The band at 400 eV is the free amine and the band at 402 is the protonated amine.[27] (e) The optical micrograph of spin-coated chitosan film on pre-fabricated Pd protodes. (f) The I–V curve of chitosan film from 70% TFA-30% DCM solution (orange curve) and from 30% acetic acid (black curve) acquired in an atmosphere comprising flowing 10% H_2 / 90% N_2 at 75% RH.

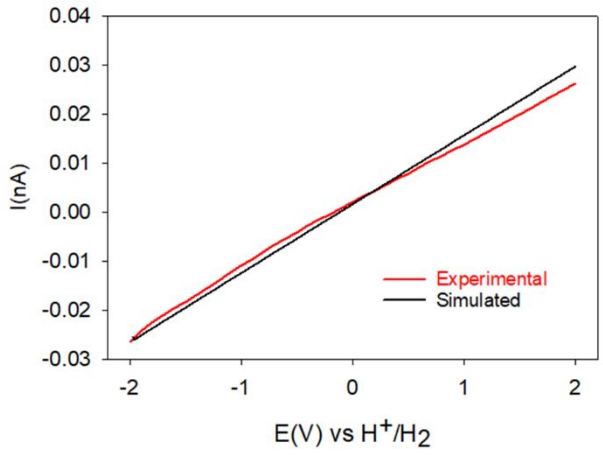

Fig. 4. Digital simulation of the proton conductivity of single chitosan fiber; experimental data (black) and digital simulation (red).

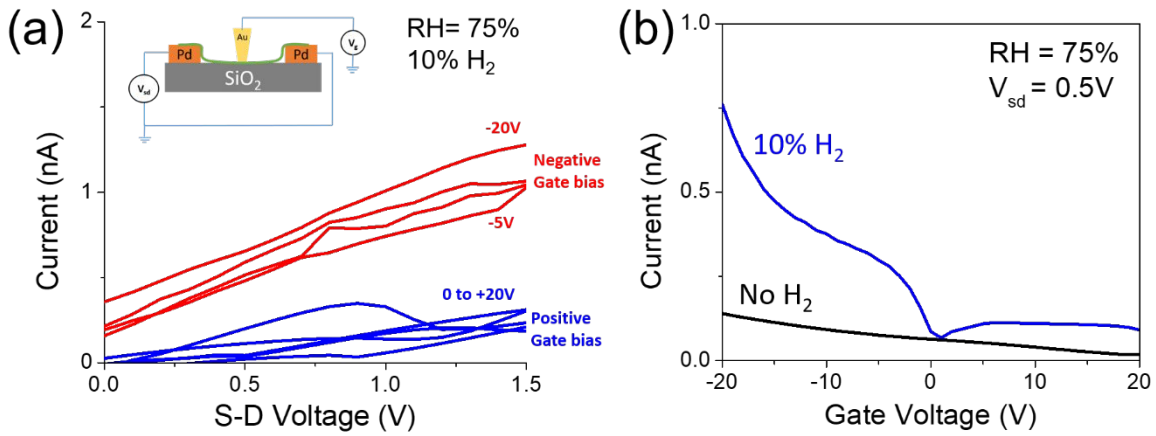

Fig. 5. The measurement of top-gated, single chitosan fiber ionic field effect transistor (IFET). The schematic illustration (inset) shows our measurement set-up with conductive AFM system (see Supplementary information, SI. 6). (a) I–V curve vs gate bias sweeping from -20V to +20V with 5V steps under 10% H_2 / 90% N_2 at 75% RH. (b) Source–Drain (PdH_x protodes) current measurement vs gate sweep. The field-effect on single chitosan fiber proton conduction is clearly evident under 10% H_2 (blue), absent without H_2 (black).

Device	**L x W (µm)**	**A_1 (cm^2) (contact)**	**A_2 (cm^2) Cross-sectional**	**Gap length (µm)**	**R (Ω)**	**ρ (Ω·cm) $R \cdot A_2/L$**	**σ = 1/ ρ $S \cdot cm^{-1}$**	**k^o (cm s^{-1})**
1	5.1 × 0.36	1.8×10^{-8}	1.0×10^{-9}	4.5	5×10^{10}	9.8×10^{4}	1×10^{-5}	2×10^{-5}
2	3.4 × 0.264	9.0×10^{-9}	5.5×10^{-10}	6.7	3×10^{10}	2.4×10^{4}	4.1×10^{-5}	2×10^{-5}
3	3.1 × 0.569	1.8×10^{-8}	2.5 x 10^{-9}	10	7×10^{10}	1.8×10^{5}	5.6×10^{-6}	2×10^{-5}
4	2.05 × 0.55	1.1×10^{-8}	2.4×10^{-9}	22.4	5.5×10^{10}	5.8×10^{4}	1.7×10^{-5}	2×10^{-5}

Table I. Conductivity data and electrochemical rate constants of four different single chitosan fibers

Table of Contents

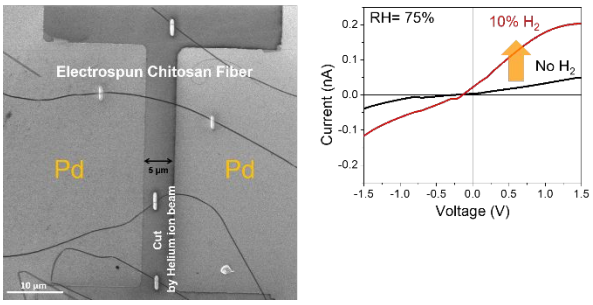

Enhanced proton transfer of electrospun, single chitosan fiber doped by TFA under the presence of hydrogen in 75% relative humidity